Chapter 3

A Low Resolution Recombination Line Survey – Observations and Basic Results

3.1 Introduction

That low-density ionized gas is present in the galactic disk is evident from several observations carried out in the past (see Section 1.3). In the radio spectral regime, this component is mostly studied by observing low frequency (< few GHz) hydrogen RRLs originating from this ionized component. Although several RRL surveys of the galactic plane have been made, many questions remain unanswered. For example, the distribution of ionized gas and its association with other components of the ISM are not well known. Also, the physical properties are estimated only towards a selected set of directions and are not well constrained, especially the temperature and size. The origin of low-density ionized gas is still a controversy. Part of the difficulty in answering these questions is due to a lack of complete sampling of the ionized gas in the galactic disk. Secondly, most of the existing RRL surveys are at only one frequency near 1.4 GHz. To determine the physical properties of the line emitting gas, RRL observations at more than one frequency are essential.

With the objective of understanding the distribution of ionized gas, its association with other components of the ISM, and to constrain its physical properties we surveyed the RRL emission in the galactic plane near 327 MHz using the ORT. Large scale surveys of RRLs at a low frequency are extremely time consuming since line emission is very weak ($10^{-3}\times$ the continuum temperature). In fact, low frequency RRLs are some of the weakest spectral lines observed in Astronomy. From earlier studies, it is known that the clouds producing RRL emission have large angular extent (see Section 1.3). This fact is made use of here to survey a large area of the galactic plane in a reasonable observing time with a coarse beam. The loss in sensitivity of the observations due to the larger beam is not significant since the line emitting regions are extended thus filling a considerable fraction of the beam. The RRL survey described in this chapter was made with an angular resolution of $\sim 2^\circ \times 2^\circ$. Although the angular resolution is coarse, these observations represent the first contiguous survey of recombination line emission in the longitude range $l = 332^\circ$ to 0° to 89°. The details of the observations are discussed in Section 3.2 and results in Section 3.3.

3.2 Observations

The RRL survey was made using a part of the ORT, called a 'module', which effectively forms a telescope of size 24 m $\times$ 30m. The observations were made in Mode A, which is described in Section 2.4.1. In this mode, we observed eight spectra simultaneously, which corresponds to four RRL transitions from two modules of the ORT. The observed recombination lines are 270α, 271α, 272α and 273α transitions of hydrogen and carbon. The modules were selected such that they have 'good' sensitivity and the baseline length between the two modules was more than $\sim$ 300 m (see Section 2.8). We found that the signals from modules near the control room were affected by narrow band interferences, mainly due to computers, modem etc. and hence these modules were not used for the observations. To reduce interference from the observatory further, instruments that were potential sources of interferences and unused computers were switched off during the observing sessions.

The declination coverage of the module is $\sim \pm$ 50°. This limitation arises from the characteristics of the dipole array (see Section 2.2), which forms the primary feed of the ORT. The limited declination coverage constraints the observations in the galactic plane to two longitude ranges. These ranges are l = 332° to 0° to 89°, which is towards the galactic center direction – mostly the first quadrant, and l = 172° to 252°, which is in the galactic anticenter direction – mostly in the fourth quadrant. The observations can be broadly classified into three categories.

1. *The Inner Galaxy :* In this thesis we refer to the longitude range l = 332° to 0° to 89° as the inner Galaxy. In this longitude range we have conducted an unbiased contiguous sampling of the galactic plane. A total of 51 spectra each separated in longitude by $\sim 2° \times \sec(\delta)$, δ being the declination, and at $b = 0°$ were taken.

2. *The Outer Galaxy :* A total of 14 positions equally spaced in longitude were observed in the range $172° < l < 252°$. This longitude range was coarsely sampled since earlier observations had indicated that low frequency RRLs are not widely detected in the outer Galaxy (Anantharamaiah 1985a).

3. *Scans along Galactic Latitude :* At two specific longitudes in the inner Galaxy (l = 0.0° & 13°.9), spectra were taken in steps of 1° up to $b = \pm 4°$ to study the latitude extent of the ionized gas.

Along with spectral measurements, we also measured the system temperature and continuum antenna temperature towards the observed positions. The system temperature is required to convert the spectral estimate in terms of antenna temperature. This conversion is required since the spectral estimates are obtained with a one-bit autocorrelation spectrometer (see Section 2.3), which gives a normalized spectrum. The continuum measurements were made as described in Section 2.7 and are tabulated in Table 3.1.

3.3 Results

The recombination line spectra observed in the inner Galaxy are shown in Fig. 3.1a. The spectra from the outer Galaxy and those obtained at different latitudes are shown in Fig. 3.1b, c & d. All the spectra are plotted in units of line to continuum temperature

Table 3.1: Summary of the RRL survey near 327 MHz

l (°)	b (°)	T_L/T_C × 10^3	T_L (mK)	ΔV (km s^{-1})	V_{LSR} (km s^{-1})	V_{res} (km s^{-1})	RMS[1] × 10^3	t_{int} (hrs)	T_C[2] (K)	Note
				Inner Galaxy						
332.1	+0.0	0.79(0.04)	133(7)	47.8(2.7)	−58.4(1.1)	8	0.22	7.6	257	h
334.9	+0.0					8	0.21	9.9	259	
337.7	+0.0	0.60(0.03)	133(6)	23.1(1.1)	−48.3(0.5)	8	0.17	9.1	341	h
340.3	+0.0	0.59(0.02)	120(4)	54.1(2.4)	−36.3(1.0)	8	0.14	10.0	313	h
342.9	+0.0					8	0.22	7.8	325	
345.5	+0.0	0.78(0.04)	188(9)	34.2(1.8)	−16.0(0.8)	8	0.18	8.2	371	h
		0.42(0.05)	101(12)	19.2(2.6)	−170.9(1.1)					c
348.0	+0.0	0.58(0.03)	148(7)	53.6(2.9)	−22.6(1.2)	8	0.19	12.7	395	h
350.4	+0.0	0.89(0.03)	221(7)	35.3(1.4)	−14.0(0.6)	8	0.14	13.3	380	h
352.9	+0.0	0.91(0.02)	288(7)	42.6(1.2)	−13.6(0.5)	8	0.14	11.9	490	h
355.3	+0.0	0.64(0.05)	216(17)	13.4(1.2)	2.2(0.5)	5	0.16	17.0	519	h
357.6	+0.0	0.63(0.05)	291(23)	26.2(2.4)	−1.2(1.0)	3	0.21	8.0	714	h
		0.47(0.05)	216(25)	22.2(3.0)	−158.7(1.3)					c
0.0	+0.0	0.94(0.04)	663(28)	29.0(1.4)	5.9(0.6)	5	0.17	11.4	1085	h
		0.42(0.04)	296(27)	29.2(3.1)	−146.8(1.3)					c
2.3	+0.0	0.46(0.03)	209(14)	26.0(2.0)	10.2(0.8)	6	0.13	10.7	699	h
		0.55(0.04)	247(17)	16.1(1.3)	−143.2(0.6)					c
4.7	+0.0	0.90(0.03)	379(13)	28.8(1.2)	11.3(0.5)	5	0.15	13.1	644	h
		0.76(0.06)	318(24)	8.5(0.7)	−142.6(0.3)					c
7.0	+0.0	0.78(0.06)	347(27)	24.8(2.2)	20.6(0.9)	5	0.25	7.2	685	h
		0.64(0.08)	283(37)	12.1(1.9)	−141.6(0.8)					c,t
9.3	+0.0	0.63(0.02)	255(10)	33.9(1.5)	19.6(0.6)	8	0.12	14.9	624	h
		0.49(0.03)	198(11)	23.5(1.5)	−126.7(0.6)					c
11.6	+0.0	0.70(0.02)	269(8)	43.0(1.5)	27.2(0.6)	8	0.14	12.6	591	h
13.9	+0.0	1.20(0.04)	513(18)	38.1(1.5)	26.9(0.6)	2	0.21	16.9	657	h
		0.74(0.11)	317(45)	6.0(1.0)	−131.8(0.4)					c,t
16.1	+0.0	1.02(0.03)	375(10)	46.6(1.4)	28.8(0.6)	3	0.15	16.8	568	h
		0.53(0.06)	197(21)	10.7(1.3)	−127.4(0.6)					c
18.4	+0.0	0.77(0.03)	299(13)	30.6(1.6)	30.0(0.7)	6	0.16	10.8	599	h
		0.36(0.05)	141(18)	17.3(2.5)	−125.5(1.1)					c
20.7	+0.0	0.40(0.03)	142(12)	34.2(3.4)	55.2(1.4)	8	0.17	11.6	540	h
23.0	+0.0	0.57(0.02)	217(9)	50.6(2.4)	70.2(1.0)	8	0.13	15.1	588	h
25.2	+0.0	0.61(0.03)	221(10)	26.0(1.4)	97.3(0.6)	8	0.13	19.9	554	h
27.5	+0.0	0.55(0.02)	183(8)	28.5(1.4)	91.6(0.6)	8	0.11	18.1	513	h
		0.39(0.03)	130(10)	16.9(1.5)	−52.6(0.6)					c
29.7	+0.0	0.88(0.02)	291(8)	36.2(1.1)	92.2(0.5)	8	0.13	17.7	510	h
32.0	+0.0	0.82(0.02)	227(7)	31.7(1.1)	91.2(0.5)	8	0.12	15.0	424	h
34.2	+0.0	0.34(0.02)	117(6)	14.2(0.9)	45.6(0.4)	5	0.10	38.4	524	h,t
36.5	+0.0	0.41(0.02)	107(4)	60.0(3.2)	65.2(1.2)	8	0.11	33.5	407	h
38.7	+0.0					8	0.11	27.6	392	
40.3	+0.0					8	0.18	21.8	361	
41.0	+0.0	0.26(0.02)	59(5)	36.3(3.8)	55.1(1.6)	8	0.12	20.7	348	h
		0.21(0.02)	47(5)	36.5(4.7)	−104.8(2.0)					c
43.2	+0.0					8	0.10	26.7	307	
45.5	+0.0	0.35(0.02)	60(3)	40.5(2.2)	48.8(0.9)	8	0.08	53.5	267	h
47.8	+0.0					8	0.15	26.1	267	
50.0	+0.0	0.30(0.02)	52(3)	58.3(4.3)	50.5(1.7)	8	0.11	45.3	268	h
		0.24(0.03)	42(6)	16.5(2.6)	−100.2(1.1)					c,t
52.3	+0.0	0.43(0.03)	54(3)	31.7(2.4)	49.6(1.0)	8	0.15	35.5	190	h
54.6	+0.0	0.42(0.03)	41(3)	14.2(1.3)	31.4(0.6)	5	0.17	48.5	150	h,t
56.9	+0.0	0.60(0.04)	45(3)	21.2(1.6)	20.9(0.7)	8	0.17	46.2	116	h
59.2	+0.0	0.55(0.04)	39(3)	21.0(2.0)	25.2(0.8)	8	0.16	22.3	109	h
		0.55(0.04)	39(2)	33.9(2.4)	−129.8(1.0)					c

Table 3.1: *Continued*

l (°)	b (°)	T_L/T_C × 10^3	T_L (mK)	ΔV (km s^{-1})	$V_{\rm LSR}$ (km s^{-1})	V_{res} (km s^{-1})	RMS[1] × 10^3	t_{int} (hrs)	T_C[2] (K)	Note
61.5	+0.0	0.57(0.02)	38(2)	34.9(1.8)	29.4(0.8)	8	0.16	52.0	104	h
63.8	+0.0	0.66(0.06)	38(4)	14.7(1.6)	22.6(0.7)	5	0.26	39.4	88	h
66.2	+0.0					8	0.20	45.2	83	
68.6	+0.0					8	0.19	40.8	91	
70.9	+0.0	0.99(0.04)	65(3)	28.9(1.3)	86.2(0.6)	8	0.25	26.4	101	h,t
73.3	+0.0	0.54(0.04)	30(2)	29.1(2.3)	22.6(0.9)	6	0.21	47.1	86	h,t
75.8	+0.0	0.65(0.03)	45(2)	39.9(2.3)	3.4(1.0)	8	0.17	35.8	105	h
		0.39(0.04)	27(2)	33.5(3.4)	−121.5(1.5)					c
78.2	+0.0	1.05(0.02)	125(3)	35.1(1.0)	3.1(0.4)	8	0.13	26.9	183	h
		0.46(0.03)	55(3)	31.6(2.1)	−154.4(0.9)					c
80.7	+0.0	1.18(0.03)	142(4)	28.5(0.9)	4.1(0.4)	8	0.15	15.2	185	h
		0.53(0.04)	64(4)	21.3(1.7)	−143.9(0.7)					c
83.3	+0.0	1.03(0.04)	75(3)	37.8(1.6)	3.8(0.7)	8	0.22	13.0	113	h
85.9	+0.0					8	0.35	21.4	66	
88.6	+0.0					8	1.03	13.2	28	
				Outer Galaxy						
172.8	+0.0					2	0.54	26.9	58	
179.6	+0.0	1.48(0.20)	16(2)	24.4(3.8)	2.6(1.6)	8	0.66	46.4	17	h
184.3	+0.0					8	0.37	29.8	53	b
191.2	+0.0					8	0.20	36.5	75	
195.8	+0.0					8	0.32	30.6	70	
202.6	+0.0					8	0.37	20.3	61	
207.1	+0.0	0.87(0.07)	45(4)	21.7(2.1)	20.1(0.9)	6	0.31	23.3	80	h
213.8	+0.0					8	0.29	23.1	65	
218.3	+0.0					8	0.38	27.4	55	b
225.1	+0.0					8	0.52	11.4	55	b
229.7	+0.0					8	0.37	31.9	56	b
236.5	+0.0					8	0.41	18.4	55	b
241.1	+0.0	1.22(0.08)	43(3)	24.5(1.9)	6.0(0.8)	8	0.33	22.0	54	h
252.9	+0.0					8	0.29	27.5	55	
				Observations along Galactic latitude						
0.0	−4.0					8	0.11	21.1	278	
0.0	−3.0					8	0.12	18.2	373	
0.0	−2.0	0.43(0.02)	164(10)	22.1(1.6)	2.2(0.7)	5	0.11	24.8	593	h
		0.35(0.04)	135(15)	10.0(1.3)	−138.0(0.5)					c
0.0	−1.0	0.82(0.02)	530(14)	28.9(0.9)	0.5(0.4)	3	0.10	25.1	998	h
		0.45(0.02)	291(15)	25.4(1.5)	−145.0(0.6)					c
0.0	+1.0	0.96(0.02)	449(12)	24.9(0.8)	3.4(0.3)	5	0.10	23.7	721	h
		0.61(0.03)	287(13)	19.6(1.0)	−146.9(0.4)					c
0.0	+2.0	0.35(0.02)	108(7)	23.3(1.7)	5.2(0.7)	8	0.09	23.2	482	h
		0.32(0.02)	99(6)	33.7(2.2)	−148.6(0.9)					c
0.0	+3.0					3	0.19	27.2	344	
0.0	+4.0					5	0.18	25.1	254	
13.9	−3.0	0.34(0.03)	71(5)	42.0(4.0)	23.4(1.6)	6	0.15	16.9	207	h
13.9	−2.0	0.47(0.03)	125(8)	40.1(3.1)	27.4(1.3)	8	0.14	20.0	269	h
13.9	−1.0	0.72(0.02)	275(7)	49.5(1.4)	31.1(0.6)	8	0.11	21.1	384	h
13.9	+1.0	1.01(0.02)	361(8)	48.8(1.2)	30.4(0.5)	5	0.16	21.3	358	h
13.9	+2.0	0.74(0.02)	193(6)	30.9(1.1)	23.2(0.5)	6	0.12	19.7	260	h
13.9	+3.0					6	0.14	20.8	207	

1) RMS is in units of T_L/T_C

2) Continuum temperature is the measured antenna temperature divided by 0.65, which is the beam efficiency factor. The error in these measurements is ± 10%.

Note: h denotes hydrogen line, c denotes carbon line, t for tentative detection, b for blank region.

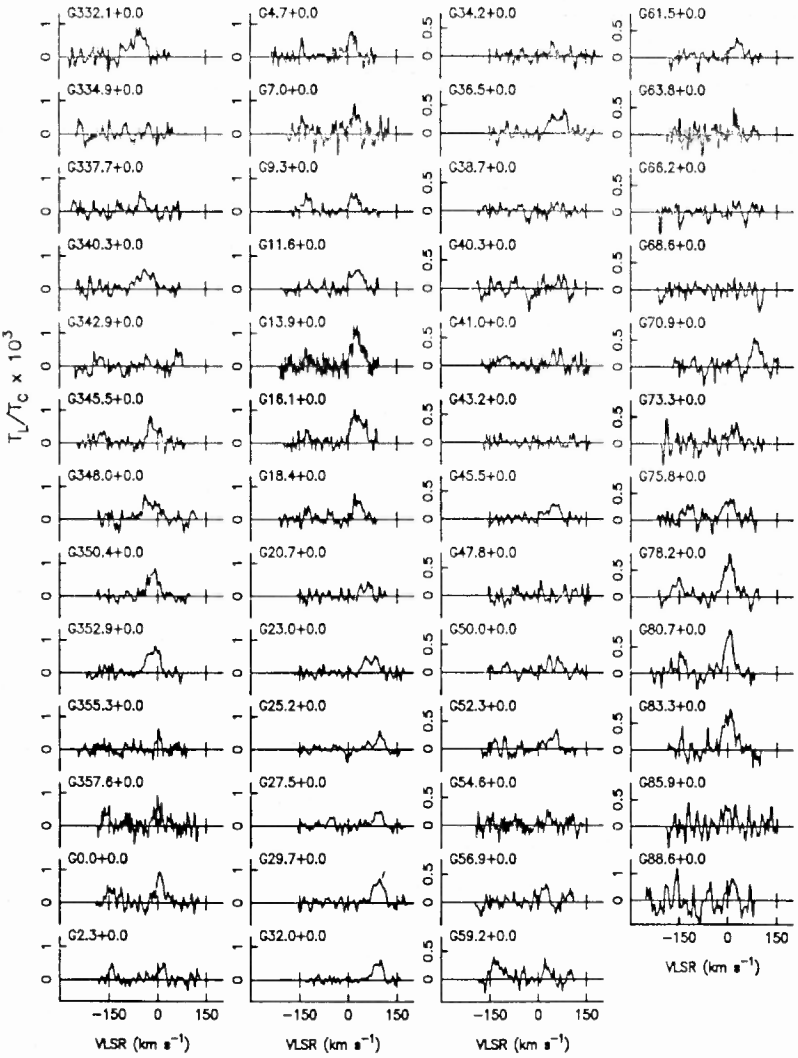

Figure 3.1: (a) Spectra observed towards the inner Galaxy. The galactic coordinates of the observed positions are marked in each spectrum. The ordinate of the spectra is in line to continuum ratio (T_L/T_C) and the abscissa is in LSR velocity. Note that the ordinate scale of spectra in each column is different.

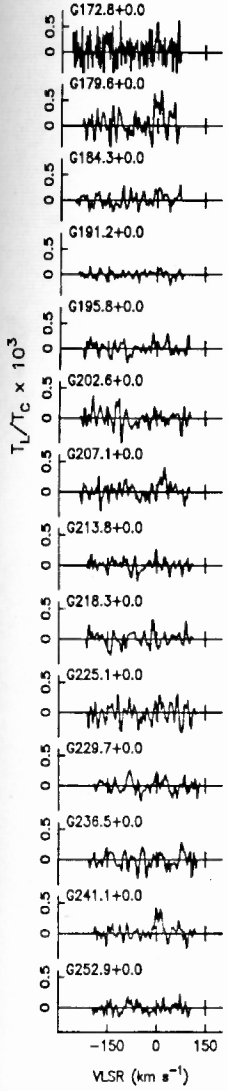

Figure 3.1: (b) Spectra observed towards the outer Galaxy. The galactic coordinates of the observed positions are marked in each spectrum. The ordinate of the spectra is in line to continuum ratio (T_L/T_C) and the abscissa is in LSR velocity.

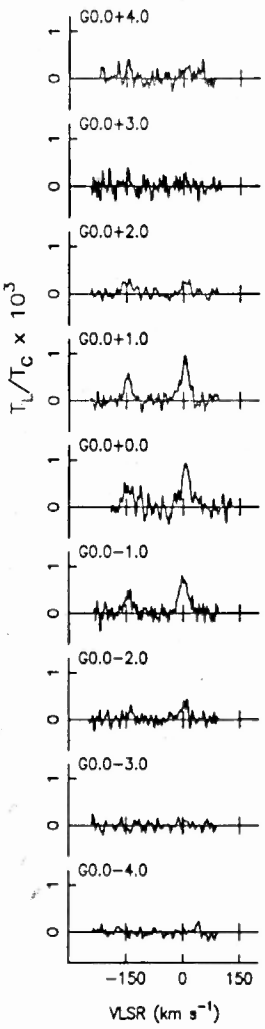

Figure 3.1: (c) Spectra observed along galactic latitude at $l = 0°.0$. The galactic coordinates of the observed positions are marked in each spectrum. The ordinate of the spectra is in line to continuum ratio (T_L/T_C) and the abscissa is in LSR velocity.

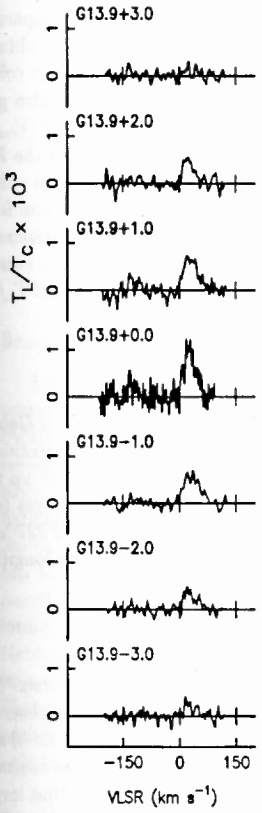

Figure 3.1: (d) Spectra observed along galactic latitude at $l = 13°.9$. The galactic coordinates of the observed positions are marked in each spectrum. The ordinate of the spectra is in line to continuum ratio (T_L/T_C) and the abscissa is in LSR velocity.

ratio (T_L/T_C) against the LSR (local standard of rest) velocity computed with respect to the rest frequency of the H272α transition. They are smoothed to the velocity resolution given in column 7 of Table 3.1. In many of the spectra, two emission features are detected. The feature closer in velocity to 0 km s^{-1} is the hydrogen line and the feature which is about -150 km s^{-1} from hydrogen is most likely a carbon recombination line. All the line features detected in this survey are in emission.

Table 3.1 gives the parameters derived from the spectra. The galactic coordinates of the observed positions are given in column 1 and 2. The ratio of the observed line temperature to continuum temperature (T_L/T_C), the peak line antenna temperature (T_L), the width (FWHM) of the line (ΔV) and the central velocity ($V_{\rm LSR}$) obtained from a single Gaussian fits to the hydrogen and the carbon lines are given in column 3, 4, 5 and 6 respectively. 1σ errors obtained from the Gaussian fits are also given along with the derived parameters. Column 7 gives the velocity resolution (V_{res}) to which the spectra shown in Fig. 3.1a–d were smoothed and column 8 gives the RMS noise of the residual spectrum obtained after subtracting the fitted Gaussian in units of T_L/T_C. The effective integration time (t_{int}) of each spectrum is given in column 9 and the measured continuum temperature is given in column 10. The notes corresponding to different symbols in column 11 are given at the bottom of the Table. On the average, the integration time for each position is $\sim$ 20 hrs and the RMS noise (in units of T_L/T_C) is typically 1.5 $\times$ 10^{-4}.

3.3.1 Hydrogen Line

RRLs of hydrogen were detected in $\sim$ 80% of the observed positions in the inner Galaxy. On the other hand, only three out of the 14 observed positions yielded detection in the outer Galaxy. The observations along the galactic latitude detected lines up to b $\sim$ $\pm3^\circ$ (Fig. 3.1c&d). The line to continuum ratio of the hydrogen line ranges from 0.3×10^{-3} to 1.4×10^{-3}. These values are comparable to T_L/T_C observed near 327 MHz by Anantharamaiah (1985a, b) using a beam of $2^\circ \times 5'.5$. The lines in the longitude range $l = 50^\circ$ to 70° are detected for the first time.

Line Width

Fig. 3.2a shows the distribution of the observed widths of the hydrogen line. The median is 31.3 km s^{-1}. These line widths are larger than the typical line widths observed from both "compact" (Downes et al. 1980, Caswell & Haynes 1987, Lockman 1989) and "diffuse" H II regions ($\sim$ 26 km s^{-1}) (Lockman et al. 1996). Comparing the observed line widths with those found in earlier surveys at higher frequencies, we find that larger line widths ($>$ 30 km s^{-1}) are more frequent in the present observations. At 327 MHz, the line widths can be affected by pressure broadening if the densities are higher than 30 cm^{-3} (Shaver 1975). However, the estimated densities (see Chapter 5) are too low for this effect to be significant. It is possible that the large line widths are due to blending of lines at different central velocities within the $2^\circ \times 2^\circ$ beam. A few of the positions (e.g. G355.3+0.0) show narrow hydrogen lines ($\sim$ 14 km s^{-1}). Such narrow lines were earlier observed from some normal H II regions (Shaver, McGee & Pottasch 1979, Lockman 1989, Lockman et al. 1996). Upper limit for the temperature of the ionized gas obtained from the width of these narrow lines is $\sim$ 4300 K.

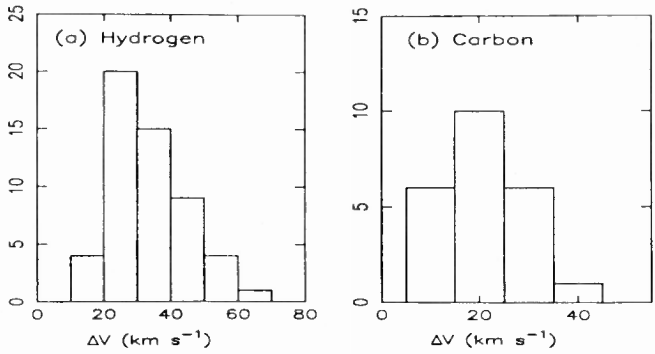

Figure 3.2: Histogram of the widths of the observed lines: (a) hydrogen (b) carbon.

Stimulated Emission

Fig. 3.3a shows a plot of the line antenna temperature near 327 MHz against the corresponding continuum antenna temperature at the observed positions. Since the continuum temperature at these frequencies is dominated by the galactic non-thermal emission, the observed correlation (correlation coefficient = 0.88) implies stimulated emission. The line to continuum ratio at these frequencies is approximately the line optical depth. Since the line optical depth is a function of the physical properties of the ionized gas producing the line (Shaver 1975), the scatter of the data points in Fig. 3.3a can be partly due to different physical properties of ionized gas in different directions. Another effect which can also contribute to this scatter is the different distances to the ionized gas, which changes the foreground contribution to the continuum temperature. Nevertheless, Fig. 3.3a is a clear indication of the dominance of stimulated emission. The importance of stimulated emission of RRLs at low frequencies was discussed earlier by Shaver (1975). It was observed towards the galactic center region by Pedlar et al. (1978) and Roshi & Anantharamaiah (1997) and in the galactic plane by Anantharamaiah (1985a).

Integrated Line Intensity vs Galactic Longitude

The velocity-integrated line intensity of hydrogen line emission and continuum intensity, both obtained with a beam of $\sim 2^\circ \times 2^\circ$ at 327 MHz, are plotted as a function of longitude in Fig. 3.4. While the continuum intensity shows a smooth variation with longitude, the line emission shows large fluctuations. These fluctuations imply that the line emitting region is not a uniform homogeneous medium, even after smoothing over 2°. The prominent peaks in RRL emission are at longitudes $l = 0^\circ$ and $l \sim 15^\circ$. The enhanced line and continuum emissions near $l = 80^\circ$ are associated with the well known Cygnus complex.

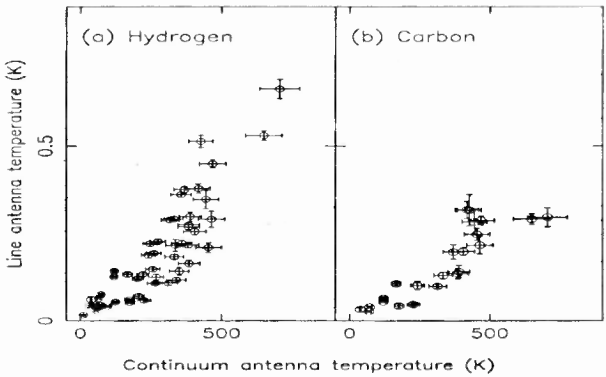

Figure 3.3: The line antenna temperature observed at different positions are plotted against the measured continuum antenna temperature at the corresponding positions: (a) hydrogen (b) carbon.

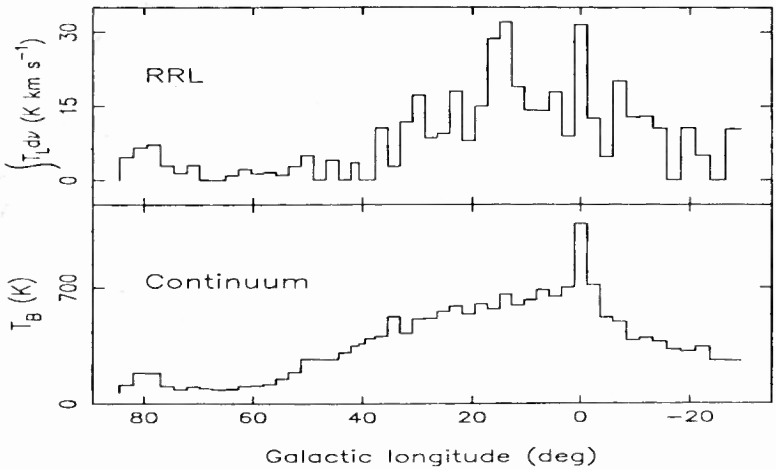

Figure 3.4: The velocity integrated line intensity of hydrogen line (top) and the continuum brightness temperature (bottom) near 327 MHz at different galactic longitude in the inner Galaxy are shown in the plot.

3.3.2 Carbon Line

The emission feature seen at about -150 km s^{-1} with respect to the hydrogen line in several spectra in Fig. 3.1a–d is most likely due to carbon. The line to continuum ratio of the carbon line ranges from 0.3×10^{-3} to 1.7×10^{-3}. The line to continuum ratio at some of the positions are comparable to or even more than that of the hydrogen line. The distribution of the width of the observed carbon lines are shown in Fig. 3.2b. Widths of the carbon lines vary over a wide range; 6.0 km s^{-1} to 37 km s^{-1} . A plot of the carbon line intensity against the continuum emission at the corresponding position (Fig. 3.3b) shows good correlation (correlation coefficient = 0.88), indicating the presence of stimulated emission.

The reason that the carbon line is almost as strong as the hydrogen line in spite of the small C/H abundance ratio in the ISM ($< 3 \times 10^{-4}$), is that the two lines arise in regions with different physical properties. While the hydrogen line arises in hot (T$\sim 10^4$ K) fully ionized regions, the carbon lines originate in cooler (T$\sim$ 100 K) partially ionized regions. In these regions only carbon is fully ionized due to its lower ionization potential. Two types of regions are known to produce carbon recombination lines. The first type is the C II regions which surround the ionization bound H II regions where carbon is ionized by the lower energy (11.4 eV $<$ E $<$ 13.6 eV) photons from the exciting star. Narrow (few km s^{-1}) carbon RRLs from such regions are typically detected at frequencies higher than 1 GHz (Pankonin et al. 1977, Kantharia, Anantharamaiah, & Goss 1998). To our knowledge no Carbon RRLs from such regions have been detected at 327 MHz. The second type of regions that generate RRLs of carbon are the diffuse HI or molecular clouds in which carbon is ionized by the background UV radiation. Very low frequency (26 MHz) RRLs of carbon from such regions were first detected in absorption by Konovalenko & Sodin (1980). Carbon RRLs from such regions were shown to appear in emission above 200 MHz (Payne, Anantharamaiah & Erickson 1989, Kantharia, Anantharamaiah and Payne 1998). Such lines are now known to be widespread in the inner Galaxy (Erickson, McConnell & Anantharamaiah 1995, Roshi & Anantharamaiah 1997, Kantharia & Anantharamaiah 1999). The carbon lines seen in Figs. 3.1a–d most likely belong to this latter category. We defer further discussion of the carbon lines from this survey to a future publication.

3.4 Summary

In this chapter we have presented the observations and results of a survey of RRLs in the galactic plane near 327 MHz. The angular resolution of the observations is $\sim 2^\circ \times 2^\circ$. We made a contiguous sampling of the longitude range $l = 332^\circ$ to 0° to 89° (inner Galaxy). Although the angular resolution is coarse, these observations represent the first contiguous survey of RRL emission in this longitude range. Hydrogen RRLs were detected in almost all directions in the inner Galaxy and carbon lines in several of the positions. In the outer Galaxy ($l = 172^\circ$ to 252°), an unbiased set of 14 positions, equally spaced in longitude, were observed and lines were detected only towards 3 of them. To study the latitude extent, we observed RRLs along the galactic latitude at two specific longitudes ($l = 0^\circ.0$ & $13^\circ.9$). RRLs were detected up to $b = \pm 3^\circ$. This data will be used in the following chapters to study the distribution of the ionized gas responsible for line emission in the galactic disk and to constraint the physical properties of the ionized regions.

Chapter 4

Distribution of Low-density Ionized Gas in the Galactic Disk

In this Chapter we make use of the low resolution RRL survey data presented in the previous chapter to study the distribution of low-density ionized gas in the galactic disk. The distribution is then compared with that of other components of the ISM. The comparison is used to infer the association of low-density ionized gas with other components.

4.1 Longitude–Velocity Diagram

A longitude–velocity (lv) diagram constructed from RRL observations of the galactic plane can be used to understand the distribution of the ionized gas in the galactic disk if we make the standard assumption that the observed central velocity of the line is due to differential galactic rotation. Fig. 4.1a shows the lv diagram obtained from the present data. For comparison (which is made below) we show in Fig. 4.1b – e, the lv diagram obtained from other published spectral line data. In all the frames in Fig. 4.1, the expected lv curves for gas located at galactocentric radii 3.5 and 7 kpc are shown as dashed and dotted lines respectively. To obtain these curves and for subsequent work presented in this thesis, we have used the parameters of galactic rotation given by Burton (1988) and by Burton & Gordon (1978). These parameters are scaled to conform with the most recent IAU-recommended galactocentric distance of the Sun, $R_\odot$ = 8.5 kpc, and circular velocity at Sun, θ_0= 220 km s^{-1} (Kerr & Lynden-Bell 1986). We also show in Fig. 4.1, the lv curves expected for the four spiral arms as defined and designated by Taylor & Cordes (1993). For clarity, we have reproduced all delineations in the lv diagrams in Fig. 4.1f. It is clear from the figure that most of the line emission originate from galactocentric distances beyond 3.5 kpc. The line emission at longitudes <50° shows some confinement to the spiral arms 2 and 3. There does not seem to be much emission associated with arm 1. There is no line emission detected from the spiral arm 4 in the longitude range 20° to 89°. The central velocities of the lines detected at $l > 50°$ are close to the terminal velocities at these longitudes (see Fig. 4.1a). The large path-lengths with small velocity dispersion encountered at the tangent points probably helped in detecting these lines. The emissions in the longitude range $l = 70°$ to 85° correspond to the well known Cygnus region which is abundant in thermal gas.

The striped area shown in Fig. 4.1f (the boundary of this region is marked in

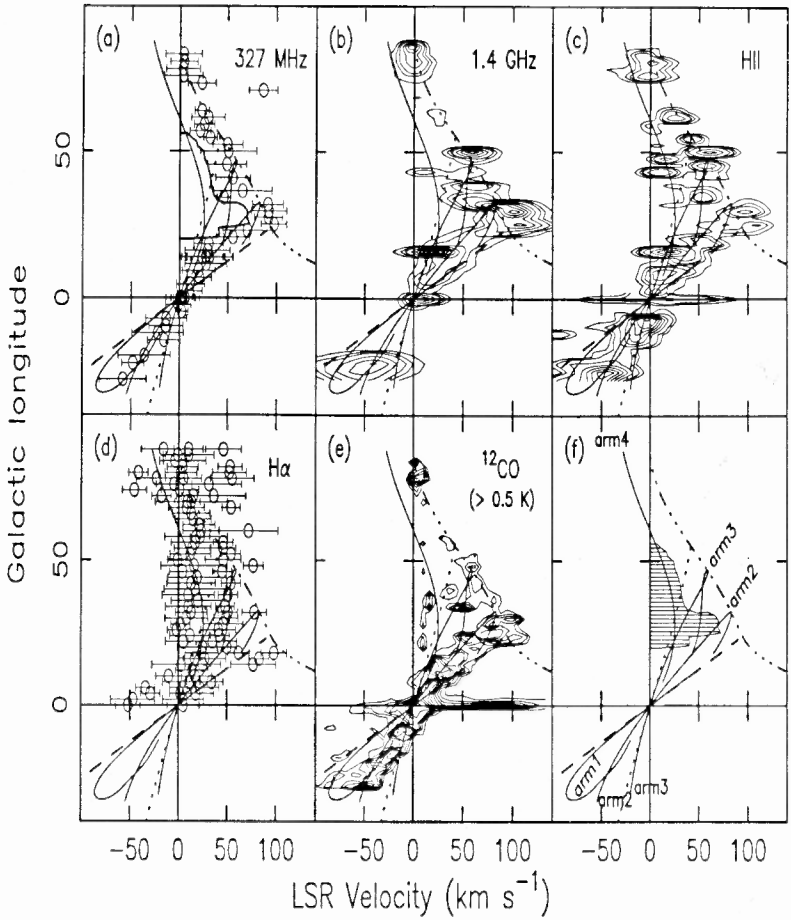

Figure 4.1: *lv* diagrams obtained from (a) 327 MHz data, (b) composite spectra of RRL emission near 1.4 GHz, (c) composite spectra of H II regions near 3 cm, (d) Hα emission and (e) "intense" ^{12}CO emission. For clarity the delineations in the *lv* diagrams are separately shown in (f). They correspond to the four spiral arms (1 to 4 as designated by Taylor & Cordes 1993), the *lv* curves corresponding to an annulus of 3.5 kpc (dashed line) and 7 kpc (dotted line) and the terminal velocity at different galactic longitude (dash-dot-dot-dot line). The striped region in (f) corresponds to a region devoid of line emission near 327 MHz (the boundary of this region is shown in (a)) in the *lv* space. The contour levels in (b) are 10, 20, 30, 50, 70, 90, 110, 130, 150 mK, in (c) are 10, 20, 30, 50,100,150,200,250, 300,400,500,600,700 mK and those in (d) are 0.5, 0.7, 0.9, 1.1, 1.3, 1.5, 1.7, 1.9, 2.1, 2.2 K. Note that the contours in (c) for $l > 2°$ are made from the 3 cm RRL emission and those for $l < 2°$ are made from the 6 cm RRL emission from H II regions.

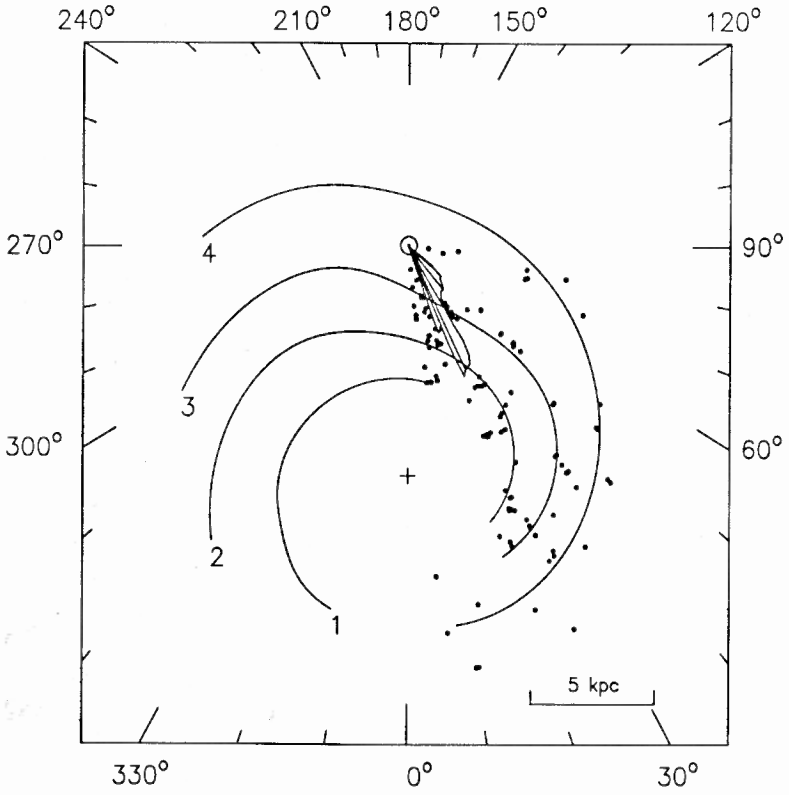

Figure 4.2: The region devoid of RRL emission near 327 MHz in the longitude-velocity space (shown in Fig. 4.1) is mapped into physical space in the galactic disk. H II regions with known distances in the longitude range 5° to 90° are marked as dots. The four model spiral arms taken from Taylor & Cordes (1989) are also shown in the figure.

Fig. 4.1a) shows a region in lv space devoid of RRL emission near 327 MHz. This region can be mapped to an area in the galactic disk by computing the near distances corresponding to the velocities bounding the shaded region. Fig. 4.2 shows this region in the galactic disk which is free of RRL emission at 327 MHz. The dots in Fig. 4.2 represent H II regions of known distances in the longitude range 5° to 90°. The H II region data is taken from Georgelin & Georgelin (1976) and Downes et al. (1980). The kinematic distances given in the data are scaled by 0.85 to conform with $R_\odot = 8.5$ kpc. The positions of the four model spiral arms are also shown in Fig. 4.2. Fig. 4.2 shows that the region devoid of RRL emission near 327 MHz is sparsely populated with H II regions. The absence of RRL emission at 327 MHz and known H II regions in this region of the galactic disk may indicate that the low-density gas detected in this survey may be associated with known H II regions. Note, however, that the H II region data with distance certainty is not complete in the longitude range 5° to 90°. In fact, the lv diagram of high frequency RRLs from H II regions do show emission in the striped region of Fig. 4.1f (Downes et al. 1980, Lockman 1989, Lockman et al. 1996). Thus there may be H II regions in the shaded region in Fig. 4.2 which do not have any low density gas associated with them. On the other hand the H II regions which occupy the striped region in Fig. 4.1f can be at the "far" distance. Thus any low-density gas associated with them are not detected in RRL emission at 327 MHz either due to beam dilution or weaker background non-thermal emission, which reduces stimulated emission.

Similarities are seen in the lv diagram shown in Fig. 4.1a with that obtained by Anantharamaiah (1985a) using the H272α line detected with a beam of 2° × 5′.5 towards selected sources in the longitude range $-2° < l < 50°$. The lower bound on the galactocentric radius of ∼ 3.5 kpc and the concentration of emission towards galactocentric radius of ∼ 5.0 kpc near the longitude 15° is evident in both the lv diagrams. However, the extension of line emission to negative velocities in the longitude range $5° < l < 20°$ seen by Anantharamaiah (1985a) is not seen in the present observations. Furthermore, in the longitude range $20° < l < 40°$ Anantharamaiah (1985a) detected line emission over a larger velocity range (10 – 150 km s^{-1}) than in the present observations (40 – 120 km s^{-1}). These differences can be ascribed to the different beams used in the two observations. The present observations were made with a beam of ∼ 2° × 2°. Thus the non-detection of some of the emission features detected in the earlier observations with a beam of 2° × 5′.5 could be because of beam dilution.

The association of the ionized gas producing RRL emission near 327 MHz with other components of the ISM in the galactic disk can be studied by comparing the lv diagram obtained for the tracers of the different components. The ionized components which are of present interest are: (1) the gas responsible for RRL emission near 1.4 GHz (Hart & Pedlar 1976b, Lockman 1976, 1980, Cersosimo 1990, Heiles et al. 1996b) which has been referred to as the ELDWIM (Petuchowski & Bennett 1993, Heiles 1994, Heiles et al. 1996b), (2) normal H II regions which are prominent in radio continuum surveys (e.g. Altenhoff et al. 1978) and which are easily detected in higher frequency RRLs (e.g. Downes et al. 1980) and (3) the distributed ionized component referred to as the WIM. A good tracer of the WIM in the local ISM is the Hα emission (Reynolds 1983). Also of interest for comparison are the distribution of the molecular component of the ISM which is obtained using the ^{12}CO line and that of the atomic component obtained from the 21 cm H I emission. Here we compare the lv diagram obtained for these different components with that from the present observations.

For the purpose of comparison of lv diagrams, we have constructed composite spectra

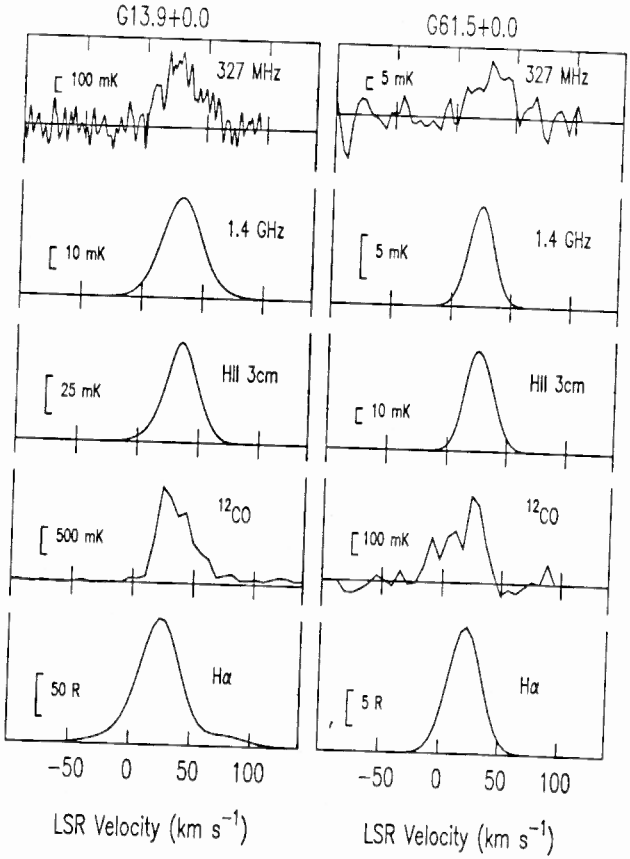

Figure 4.3: Composite spectra obtained from the spectral traces of different components of the ISM along with the 327 MHz RRL spectrum are shown for two specific longitudes, $l = 13°.9$ ($b = 0°$) and $61°.5$ ($b = 0°$). The amplitude scale for each spectrum and the spectral tracer are marked on the plot.

of different tracers by averaging the spectral emission within the 2° × 2° beam of our observations at different galactic longitude. Fig. 4.3 shows examples of composite spectra along with the line emission near 327 MHz at two longitudes, $l = 13°.9$ and $61°.5$.

RRLs near 1.4 GHz have been observed at intervals of 1° in the galactic plane by Lockman (1976, 1980) and Hart & Pedlar (1976b) and more recently at finer intervals and also at higher galactic latitudes by Heiles et al. (1996b). Near $l = 335°$ RRLs were observed at this frequency by Cersosimo (1990). The HPBW of the observations of Lockman (1976, 1980) is 21′, Hart & Pedlar (1976b) is 31′ × 33′, Heiles et al. (1996b) is 36′ (also 21′ for the observations with the 140 ft telescope) and Cersosimo (1990) is 34′. The composite spectra of RRL emission near 1.4 GHz were obtained from these data. Cersosimo (1990) and Lockman (1976,1980) have given the line intensity in antenna temperature. We have not attempted to convert them to brightness temperature for constructing the composite spectra. The *lv* diagram made from the composite spectra near 1.4 GHz is shown in Fig. 4.1b. No data near 1.4 GHz is available for the longitude range 340° to 355°. Barring this longitude range, this *lv* diagram is remarkably similar to that obtained from the 327 MHz observations (Fig. 4.1a). These similarities include (a) lack of emission at galactocentric radii less than 3.5 kpc, (b) confinement of emission in the ∼ 5.0 kpc ring in the longitude range 5° to 20°, (c) concentration of emission near the terminal velocity in the longitude range 50° to 88° and (d) lack of emission in the shaded region between $l = 20°$ to 50° except near 40°. These similarities suggest that the RRL emission observed at 327 MHz and 1.4 GHz can be attributed to the same gas. This conclusion is valuable and is used quantitatively in Chapter 5 to constrain the physical properties of the ionized gas that produces the line emission.

Fig. 4.1c shows the *lv* diagram of the composite spectra obtained from the RRL emission from H II regions. The data for this *lv* diagram are taken from extensive RRL surveys of H II regions in the inner Galaxy made by Downes et al. (1980), Caswell & Haynes (1987) and Lockman (1989). In the longitude range $2° < l < 88°$, the most sensitive and fairly well sampled survey was made by Lockman (1989) near 3cm and the composite spectra are obtained from this data. The composite spectra at longitudes $l <$ 2° are obtained from the data of Downes et al. (1980) and Caswell & Haynes (1987). These observations were made near 6 cm. The RRL emission from the H II regions are observed at higher frequencies (> few GHz) and hence originate from higher density ionized gas. Near 327 MHz, lines are not observed from such gas because of pressure broadening and large continuum opacity. The *lv* diagrams obtained from these data can be similar if the low-density gas responsible for line emission near 327 MHz are associated with the H II regions. Although the *lv* diagram of H II regions in Fig. 4.1c in general shows some similarity with that obtained from 327 MHz observations, there are many differences. The similarities include (a) lack of emission at galactocentric radii less than 3.5 kpc except near the galactic center and (b) concentration of emission near the terminal velocity in the longitude range 50° to 88°. However, in general, H II regions seem to occupy a larger space in the *lv* diagram. The H II regions show emission in the shaded region (shown in Fig. 4.1f) between $l = 20°$ to 50° and also a large velocity spread near $l = 0°$. The emission in the shaded region may be from H II region associated with arm 4 (see Fig. 4.2), which are at relatively large distances. Thus any low density gas associated with these H II regions and which could produce line emission near 327 MHz may not be detected due to large beam dilution and/or weak background continuum. In fact, the *lv* diagram constructed from observations of RRLs near 327 MHz with a

smaller beam of $2^\circ \times 5'.5$ do show some emission in the shaded region (Anantharamaiah 1985a).

The presence of a widely distributed WIM is evident from Hα (Reynolds 1983) and pulsar observations (Taylor & Cordes 1993). Comparison with the Hα observations is therefore relevant to understand any possible association of RRL emission at 327 MHz with the WIM in the inner Galaxy. Although Hα observations are far more sensitive than any RRL observations, they do not probe large line-of-sight distances due to interstellar extinction. The distinct features of the Hα line profiles are multiple components and large "wings" (Reynolds 1983). On the other hand, the line profiles of RRLs near 327 MHz do not show any evidence, within the signal-to-noise ratio, of multiple components. Our observations are not sensitive to the "wings" of the profile due to instrumental baseline uncertainties. In Fig. 4.1d we have reproduced the *lv* diagram given by Reynolds (1983) in the longitude range of interest. The Hα observations sample a field of diameter $0^\circ.82$ spaced at 2° in longitude (Reynolds 1983). Fig. 4.1d shows that, unlike RRL emission, Hα emission is present in almost all longitudes with LSR velocity ranging between 0 km s^{-1} and 60 km s^{-1} . The features detected in RRL observations beyond a velocity of 60 km s^{-1} are not seen in Hα because of large interstellar extinction. Beyond $l = 50^\circ$, the Hα emission also has components with velocities close to the terminal velocity at the corresponding longitude. It appears safe to conclude that the Hα emission observed by Reynolds (1983) and the RRLs observed near 327 MHz do not arise in the same gas.

The tracer of the molecular component of the ISM is the ^{12}CO emission. Composite spectra of ^{12}CO emission in the inner Galaxy were made from the data of Dame et al. (1987) and the *lv* diagram obtained from their data is shown in Fig. 4.1e. The velocity resolution of the composite spectra is smoothed to 6.5 km s^{-1} which is close to the typical final resolution of the data at 327 MHz. The lowest contour corresponds to an intensity level which is 25 times the typical RMS noise in the ^{12}CO spectra. These intense ^{12}CO emission corresponds to the "warm" molecular clouds discussed by Solomon, Sanders & Rivolo (1985) and are associated with star-forming regions (see below for further discussion). The *lv* diagram shown in Fig. 4.1e is remarkably similar to that obtained from the present observations except for the emission in the shaded region (shown in Fig. 4.1f) and the large velocities of ^{12}CO emission near $l = 0^\circ$. If the ^{12}CO emission in the shaded region corresponds to the "far" kinematic distance, then the RRL emission associated with them, if any, may not be detected due to reasons stated earlier, like beam dilution and/or weak continuum background. Thus we conclude that the RRL emission near 327 MHz is most likely associated with star-forming regions.

The H I emission at any longitude extends over a much larger velocity range and is significantly different from the RRL emission near 327 MHz. This has been noted earlier by Lockman (1976) and Anantharamaiah (1985a).

4.2 Distribution of the Low-density Ionized Gas as a function of R_{GC}

Although an *lv* diagram gives a qualitative understanding of the distribution of ionized gas in the galactic disk, a more quantitative study can be made by computing the average emission as a function of galactocentric radius. Since the ionized gas at "near" and "far" kinematic distance will be at the same galactocentric distance, the radial

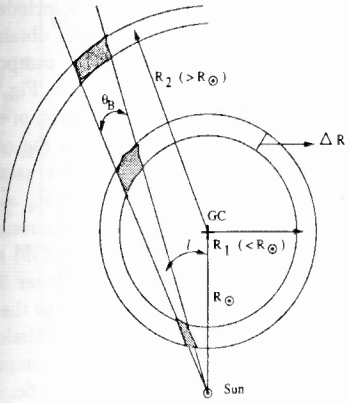

Figure 4.4: Figure shows the intersections (shaded regions) of the telescope beam (θ_B) with an annular ring of thickness ΔR centered about the galactic centre for two cases : $R_2 > \mathrm{R}_\odot$ and $R_1 < \mathrm{R}_\odot$.

distribution is not affected by the two-fold ambiguity in estimating the line-of-sight distance. However the distribution will depend on the choice of the rotation curve.

The radial distribution is obtained as follows. The galactic disk is subdivided into annuli at different galactocentric radii. Consider an annulus of radius $\mathrm{R_{GC}} = \mathrm{R}_1$ and thickness ΔR (see Fig. 4.4). R_1 is less than $\mathrm{R}_\odot$, the distance of the Sun from the galactic center. In this case, all the lines of sight with longitudes less than $\sin^{-1}(\frac{R_{GC}}{R_\odot})$ intersect the annulus at "near" and "far" distances. Near the tangent point, the two sections merge into a single one. A telescope, with a half power beam width of θ_B, receives radiation from ionized clouds situated at the two regions in the annulus shown as shaded areas in Fig 4.4. The spectral features produced by these clouds will be confined to a velocity range, say V_1 to V_2, due to differential galactic rotation. Given $\mathrm{R_{GC}}$, ΔR, the beam width (FWHM) of the telescope and a galactic rotation curve, V_1 and V_2 can be computed. The average emission (Γ) in the annulus is then given by

$$\Gamma = \frac{\sum_{l1,l2} \int_{V_1}^{V_2} T_L dv}{A_R} \tag{4.1}$$

Here the summation of the integrated line intensity is over the longitude range $l1$ to $l2$. The upper bound $|l2|$ is equal to $\sin^{-1}(\frac{R_{GC}}{R_\odot})$ if $\mathrm{R_{GC}} < \mathrm{R}_\odot$ or limited by the longitude range of observation if $\mathrm{R_{GC}} > \mathrm{R}_\odot$. For longitudes close to 0°, velocity crowding over long lines of sight makes the analysis very sensitive to the dispersion of the line profiles. Thus the computation is restricted to longitudes above a lower limit. We have used $|l_1| = 4°$ in our computation. A_R is the area of the annulus in the longitude range $l1$ to $l2$ that contributes to the observed line emission. Note that for $\mathrm{R_{GC}} > \mathrm{R}_\odot$, the telescope beam intersects only one region of the annulus. The distribution function is

then obtained by computing the average emission as a function of R_{gc} . The spectral features beyond the terminal velocity at different longitudes are not included in the computation of average emission. Fig. 4.6 shows the radial distribution obtained from the present data along with that obtained from the tracers of other components of the ISM. For the computation of all the radial distributions shown in Fig. 4.6, the galactocentric distance from 1.5 to 14 kpc was divided into annular rings of thickness 0.5 kpc. The average emission in each ring was then computed from the composite spectra of the different tracers as described above. The rotation curve used for the computation was taken from Burton & Gordon (1978) after scaling to $R_\odot = 8.5$ kpc and $\theta_0 = 220$ km s^{-1} . The computation of the distribution function was restricted to the longitude range $4° < l < 84°$ where the different components of the ISM are more or less uniformly sampled. The velocity range of the spectra observed near 327 MHz where carbon lines were present was eliminated to avoid its contribution to the average emission. In the case of H II regions, we have computed the average emission using the higher sensitivity RRL data near 3 cm by Lockman (1989). We also computed the surface density[1] of H II regions in the galactic disk and is shown in Fig. 4.6c. For this computation, the longitude range was divided into 1° bins and the data were taken from Lockman (1989) and Lockman et al. (1996). The distribution function shown in Fig. 4.6f was obtained from spectral features in the ^{12}CO emission with intensity higher than 25 times the RMS noise in the spectra. The ^{12}CO data was taken from Dame et al. (1987) and the Hα data was from Reynolds (1983). The formal errors ($\pm\ 1\sigma$) on the distribution for 327 MHz and ^{12}CO emission are also shown in the figure.

In the above calculation, it is implicitly assumed that the distribution of the ionized gas in the galactic disk is axi-symmetric. We have also not corrected for the contribution to the line width due to intrinsic velocity dispersion, which will result in smearing of the true distribution. Furthermore, there is an overlap of the velocity interval computed using the galactic rotation model for different annuli at a given longitude. This is especially so near the terminal velocities at $l < 20°$. This overlap arises due to the large beam width of our observations. Because of this overlap in the velocity range, it is not possible to assign the line emission to a unique annulus. The net effect of this overlap is an overestimation of the average emission for galactocentric distances less than 4 kpc. However, we found that the general shape of the distribution function is not significantly affected. The derived distribution could also be affected by the effect of stimulated emission due to the galactic background radiation, which may favor detection of nearby clouds. This selection effect is not taken into account here.

Another factor that could affect the shape of the radial distribution obtained from RRL emission near 327 MHz is the overlap of telescope beam towards adjacent positions observed in the low resolution survey. This is discussed below. As described in Section 2.4 the reference spectrum is obtained by switching the local oscillator frequency. In the case of the ORT this will result in a shift of the telescope beam in the sky (see Roshi 1995). The angle by which the beam shifts is a function of declination and it can be about 35% of the beam width at $\delta > 30°$. This will result in overlapping of the observed regions even though the beam centre of the selected positions are separated by the beam width. To study the effect of this overlap on the distribution function we divided the survey data into two sets. These data sets consist of spectra obtained from

[1]The surface density of H II regions are computed using the equation $\Gamma_s = \frac{\sum_{l1,l2}\sum_{v_1,v_2} N(v,l)}{A_R}$, where $N(v,l)$ is the number of H II regions in a unit LSR velocity interval.

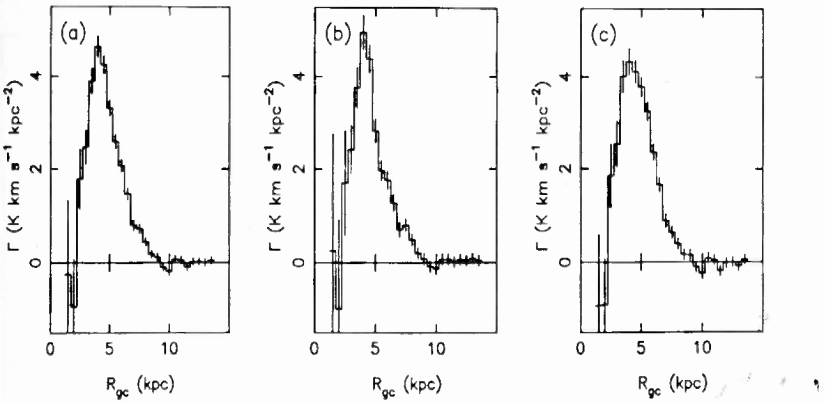

Figure 4.5: The plot of the radial distributions obtained from RRL emission near 327 MHz. (a) Distribution obtained from the entire survey data; (b) & (c) Distribution computed from the two sets of spectra that are obtained from positions separated by twice the telescope beam.

positions with beam centres separated by twice the telescope beam. The distribution functions were then computed with these sets of spectra, which are shown in Fig. 4.5 along with that obtained from the entire data. It is clear that the general features of the distribution function are not affected by the overlapping of the observed regions.

The radial distribution obtained from the 327 MHz data (see Fig. 4.6a) shows that the average emission extends from $R_{gc} = 2.5$ kpc to 9 kpc with a prominent peak near 4 kpc. Thus it is clear from the distribution that the RRLs detected in our observations do not originate in the solar neighborhood. The distribution falls quite steeply on either side of the peak, the half power width being 3 kpc. The true distribution may be narrower than this because the broadening of the distribution due to intrinsic velocity dispersion has not been accounted for. Between 7 kpc and 8.5 kpc, the average emission is less than 20 % of the peak and is near zero beyond 9 kpc. More than 70 % of the RRL emission is confined between 2.5 kpc and 6 kpc. The concentration of power in RRL emission near 4 kpc was earlier pointed out by Lockman (1976) and Anantharamaiah (1985b). (Note that the galactocentric distance to Sun is taken as 10.0 kpc in these papers and hence the peak of the distribution quoted should be scaled by 0.85.) The distribution obtained by Anantharamaiah (1986) shows emission beyond 9 kpc. This emission should arise from gas at negative velocities in the longitude range 4° to 84°. In the present observations very little emission is observed at negative velocities in this longitude range. This behavior may be attributed to the difference in the angular resolutions of the observations.

The radial distribution obtained from RRL emission near 327 MHz is very similar to that obtained from the RRL emission observed near 1.4 GHz (Fig. 4.6b). The peak of the distribution and the concentration of emission between 2.5 kpc and 6 kpc are present in both Figs. 4.6a & b. The excess emission seen near 8.5 kpc in the distribution of

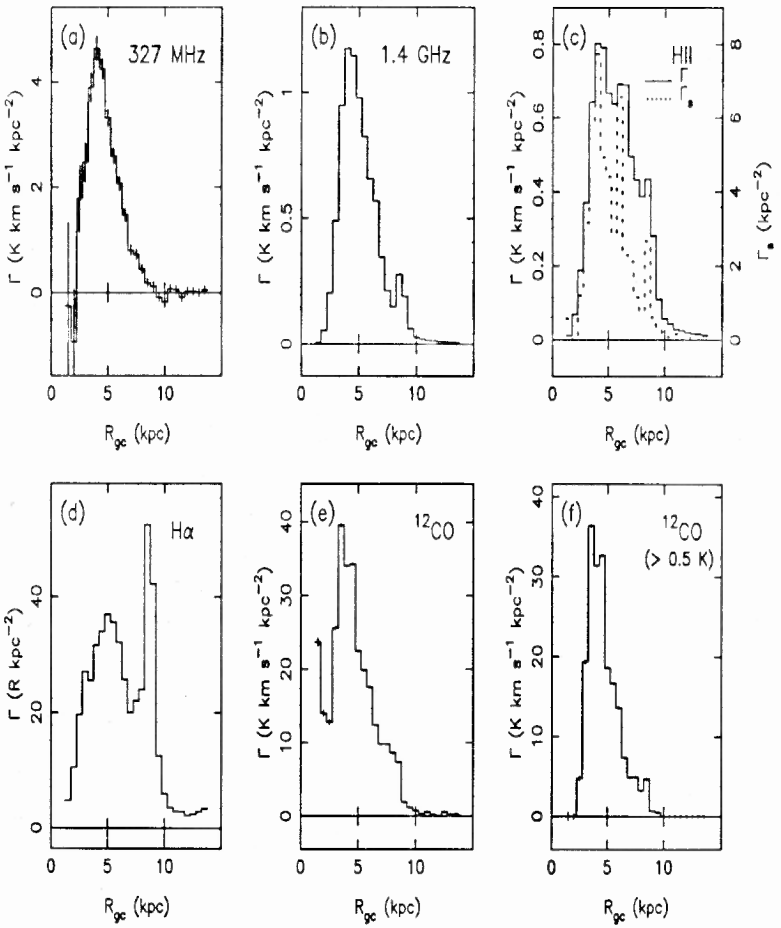

Figure 4.6: Plots of the radial distribution of different components of the ISM. They are obtained from (a) RRL emission near 327 MHz, (b) RRL emission near 1.4 GHz, (c) RRL emission from H II regions near 3 cm (solid line), (d) Hα emission, (e) ^{12}CO emission and (f) ^{12}CO spectral components of intensity higher than 0.5 K. The surface density (Γ_*) of H II regions as a function of galactocentric radius is plotted as dotted line in (c). The radial distributions were computed using the data in the longitude range $4^\circ < l < 84^\circ$ where all the components of the ISM are fairly well sampled. For the computation using the 1.4 GHz and ^{12}CO data, we have used the composite spectra.

1.4 GHz line emission is associated with thermal gas in the Cygnus region. There is no corresponding excess emission seen in the distribution obtained from the present data. The line emission near 1.4 GHz from the Cygnus region may therefore have contribution from high density H II regions which are not detected in the observations near 327 MHz. The similarity of the *lv* diagrams (Fig. 4.1a & b) and the radial distributions of RRL emission in Figs. 4.6a & b suggest that a considerable fraction of the line emission near 1.4 GHz originate in the same ionized gas that produces the line emission near 327 MHz.

The 3 cm RRL emission, which arises mostly in compact H II regions has a broader radial distribution (see Fig. 4.6c) in the range R_{gc} = 2.5 kpc to 9 kpc compared to the distribution obtained from the 327 MHz data. The distribution shows peaks near 4 kpc, 6 kpc and 8.5 kpc, which corresponds to the spiral arm structures 2, 3 (as designated by Taylor & Cordes 1993) and the local Orion arm. The emission falls quite steeply for R_{gc} < 4 kpc, similar to that seen in the distribution of RRL emission near 327 MHz. We have also computed the surface density of H II regions and is shown in Fig. 4.6c as a dotted line. For the computation of the surface density, both compact and diffuse H II region data are used. Although the surface density cannot be compared directly with the distributions obtained from line intensity, it has the advantage that RRL surveys of H II regions at different frequencies can be combined to obtain the radial distribution. The derived distribution is also not affected by the intrinsic velocity dispersion since only the central velocity is used for constructing the distribution. As expected, the surface density distribution is much narrower than the distribution of RRLs from the H II regions. The difference between the dashed and continuous curve in Fig. 4.6c gives an indication of the maximum smearing that could occur due to line width effects. Barring the peaks near 6 kpc and 8.5 kpc, the surface density distribution looks very similar to the distribution obtained from the 327 MHz data.

The radial distribution obtained from the Hα observations (see Fig. 4.6d) shows that the emission is dominated by ionized gas close to Sun. This is expected because the typical mean free path of the Hα photons is about 1 kpc. For this reason, the computed distribution shown in Fig. 4.6d does not represent the true distribution of Hα emission in the galactic disk. However it is significant that the average emission has not fallen to zero at R_{gc} < 2 kpc and the emission extends much beyond R_{gc} = 9 kpc. Thus the Hα emission is much more widespread in the inner Galaxy compared to RRL emission near 327 MHz.

Although the distribution of the molecular gas obtained from ^{12}CO emission (see Fig. 4.6e) also shows a peak near 4 kpc, there is a significant difference when compared to that of RRL emission near 327 MHz. For R_{gc} < 2.5 kpc, the average emission does not fall to zero and, in fact, the total emission increases closer to the galactic center. This increase has been discussed earlier by several authors (e.g. Combes 1991). However the distribution of the average emission of "intense" ^{12}CO emission shown in Fig. 4.6f, shows good agreement with that of RRL emission. Solomon, Sanders & Rivolo (1985) found two classes of molecular clouds in the galactic disk – "warm" and "cold". The classification is based on the observed ^{12}CO line intensity. They showed that the "warm" clouds (i.e. clouds with relatively intense ^{12}CO emission) form the spiral arm population and are associated with the H II regions. In obtaining the distribution in Fig. 4.6f, we have used composite ^{12}CO spectra and the "intense" emission were obtained by using a threshold of 0.5 K. Thus, to first order, these sites should be associated with "warm" clouds and therefore to the sites of H II regions. We may thus conclude that the

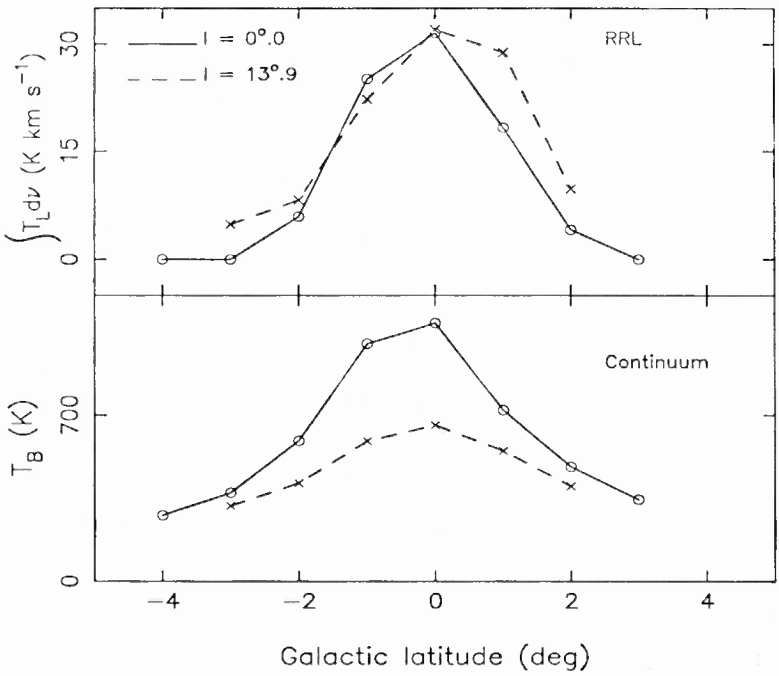

Figure 4.7: Velocity integrated recombination line intensity (top) and continuum brightness temperature (bottom) near 327 MHz are plotted against galactic latitude.

RRL emission obtained at 327 MHz in the galactic disk is associated with star forming regions.

The average emission of H I line, which samples the neutral component of the ISM, is more or less flat in the range 2.5 kpc $<$ R_{gc} $<$ 8.5 kpc and extends to distances greater than 14 kpc. Thus its distribution is distinctly different from the distribution of the RRL emission near 327 MHz as has been noted earlier by Lockman (1976) and Anantharamaiah (1986).

4.3 Latitude Extent of RRL Emission

The spectra of RRL emission as a function of galactic latitude at the two longitudes ($l = 0°.0$ & $13°.9$) are shown in Fig. 3.1c&d. RRLs have been detected upto $\pm 3°$ above the galactic plane. The latitude extent of RRL emission at 1.4 GHz observed by Heiles et al. (1996b) is similar to that seen in our observations. Fig. 4.7 shows the observed line and continuum temperatures as a function of galactic latitude. The full width at half maximum (FWHM) of the latitude extent of RRL emission is $\sim 1°.8$. A scale height (FWHM) for the emission can be derived if the distance to the line emitting region

is known. At $l = 13°.9$, the "near" and "far" distances obtained from the measured central velocity is 3 kpc and 13.5 kpc respectively. The minimum scale height implied by the "near" distance is $\sim$ 95 pc. Towards $l = 0°$, a kinematic distance to the cloud cannot be obtained. If we assume the distance to be halfway to the galactic centre, then the scale height turns out to be 133 pc. These values are close to that obtained for the molecular layer ($\sim$ 120 pc) and for the thermal gas that emits the 5 GHz continuum in the inner Galaxy (Combes 1991). The scale height of normal H II regions ($\sim$ 50 pc; Lockman et al. 1996) is about half that determined from line emission near 327 MHz.

Since, as shown in Section 3.3.1, stimulated emission is the dominant mechanism for line emission near 327 MHz, the above determination of the scale height should be regarded as a lower limit. As the background continuum decreases with latitude, the sensitivity to line emission also decreases. In fact, if we use the line to continuum ratio, which partially corrects this effect, the FWHM of line emission comes out to be $\sim 3°$.

4.4 Line Emission in the Outer Galaxy

To compare with the inner Galaxy, we observed 14 positions in the outer Galaxy ($172° < l < 252°$). The angular resolution for these observations was also $\sim 2° \times 2°$. The coordinates of the observed positions are given in Table 3.1. The observed positions were equally spaced in longitude, thus forming an unbiased sample. Five of the observed positions are devoid of any continuum source in the 2.7 GHz (Reich et al. 1990) and 408 MHz (Haslam et al. 1982) continuum surveys (see note 'b' in Table 3.1). No RRLs were detected from these positions. Of the remaining nine positions, RRLs of hydrogen were marginally detected in three positions. The observed line parameters are given in Table 3.1. No carbon lines were detected. The hydrogen line detected at the position G207.08+0.00 may be associated with the Rosette nebula which has a similar radial velocity.

These observations show that the RRL emission near 327 MHz in the outer Galaxy is not as widespread as in the inner Galaxy. Since star formation activity is less in the outer galaxy, this result supports the conclusion of the earlier section that RRL emission near 327 MHz is associated with star forming regions. However, one selection effect that may have reduced the detection rate is the lower continuum background in the outer Galaxy.

4.5 Summary

In this Chapter the low resolution RRL survey data was used to study the distribution of the low-density ionized gas in the galactic disk and its association with other components of the ISM. The *lv* diagram and the radial distribution of the RRL emission near 327 MHz and tracers of other components of the ISM are constructed for this purpose. The *lv* diagram of line emission near 327 MHz shows that most of the emission originate from galactocentric distance greater than 3.5 kpc. The line emission shows some confinement to the spiral arms at longitude $< 50°$. The measured radial velocities of the RRLs in the longitude range $50°$ to $90°$ are close to the terminal velocities of the corresponding longitude. The radial distribution of the RRL emission near 327 MHz shows a prominent peak near 4 kpc with more than 70 % of the emission originating between galactocentric radius 2.5 kpc and 6 kpc. The distribution falls steeply on either side of the peak.

The *lv* diagram and the radial distribution obtained from the present data show good agreement with that obtained from RRL emission near 1.4 GHz, "intense" ^{12}CO emission and to some extent with the distribution of RRL emission from H II regions. On the other hand, the distribution of the Hα emission and H I emission in the galactic disk is different from that of the RRL emission near 327 MHz. Thus we conclude that the RRL emission in the galactic disk is associated with the star forming regions. We also conclude that most of the RRL emission near 1.4 GHz originate from the ionized gas responsible for line emission near 327 MHz. This fact is made use in Chapter 5 to estimate the physical properties of the ionized gas producing RRL emission.

In the outer Galaxy ($l = 172°$ to $252°$) an unbiased set of 14 positions were observed in the survey and lines were detected towards 3 of them. Our observations thus show that the line emission in the outer Galaxy is not as wide spread as in the inner Galaxy. Observations along galactic latitude at two specific longitudes ($l = 0°.0$ & $13°.9$) have detected lines upto $b = \pm 3°$. We estimated a lower limit to the scale height (FWHM) of line emission from these observations as about 100 pc.